Acenes and phenacenes in their lowest-lying triplet states. Does kinked remain more stable than straight?

Ricardo Pino-Rios*[a], Rodrigo Báez-Grez[b], Miquel Solà*[c]

[a]Laboratorio de Química teórica, Facultad de Química y Biología, Universidad de Santiago de Chile (USACH). Región Metropolitana, Chile; ricardo.pino@usach.cl

[b]Computational and Theoretical Chemistry Group, Departamento de Ciencias Químicas, Facultad de Ciencias Exactas, Universidad Andres Bello. República 498, Santiago, Chile.

[c]Institute of Computational Chemistry and Catalysis, University of Girona. 17003 Girona, Catalonia, Spain; miquel.sola@udg.edu

Abstract

The larger stability of phenacenes compared to their acene isomers in their ground states is attributed to the larger aromaticity of the former. To our knowledge the relative stability of acenes and phenacenes in their lowest-lying triplet states (T_1) has not been discussed yet. Using unrestricted density functional theory calculations, our results show that for the smallests members of the series, acenes in their T_1 states are more stable than the corresponding phenacenes. However, when the number of the rings (n) involved increases, the energy difference is reduced and for n > 12, phenacenes become more stable than acenes in their T_1 states. To rationalize this trend, we analyze the aromaticity of acenes and phenacenes using a set of aromaticity descriptors. We find that in the T_1 states of both acenes and phenacenes, the outer rings form aromatic Clar π-sextets. In acenes, delocalization of spin density in the central rings leads to the preferred formation of the largest antiaromatic diradical. Resonant structures in the form of antiaromatic diradical Baird π-octadectets and π-tetradectets are the major contributors, while the smaller ones, such as π-doublets and π-sextets, contribute the least. In phenacenes, structures with diradical antiaromatic Baird π-sextets in some of the central rings contribute the most. These results are relevant to understand the (anti)aromaticity of larger polycyclic aromatic hydrocarbons in their triplet states.

Introduction

Aromaticity is a very popular property used in organic chemistry to explain the unusual stability of several cyclic conjugated compounds.[1] Although this property does not have a clear definition, aromaticity is applied in molecular design for the modulation of photoreactivity or in the development of materials for singlet fission, triplet-triplet anhilation or thermally activated delayed fluorescence among others, through the (de)stabilization of ground and excited states.[2–7] In the closed-shell singlet ground state, aromaticity obeys a series of rules[8] that allow the characterization of a compound as aromatic, non-aromatic or antiaromatic.

The most popular rule is Hückel's,[9] which states that compounds containing 4n+2 (4n) are considered aromatic (antiaromatic), the best-known example is benzene, which has 6π electrons (n = 1) and is considered the archetype of the aromatic compounds. When attempting to extend this concept to compounds with multiple rings, such as polycyclic aromatic hydrocarbons (PAHs), Hückel's rule is not applicable. For the case of benzenoid compounds, i.e. PAHs containing only six-membered rings (6MR), local aromaticity is understood qualitatively through a series of rules provided by Clar in his now classic "The aromatic Sextet".[10,11] On the other hand, in non-benzenoid compounds, the (anti)aromaticity can be characterized through the Glidewell-Lloyd rule[12] which arises as a generalization to Clar's π-sextet rule.

Acenes (PAHs with straight topology, Figure 1), and phenacenes (PAHs with kinked topology) constitute a series of isomeric PAHs families of great importance both from the theoretical point of view and in materials science, being the subject of multiple studies that have been reviewed recently.[13,14] One of the most striking features is the difference in the

stabilities between the isomers belonging to these families, with the phenacenes being more stable than the acenes. This characteristic has received several explanations based on aromaticity[15–17] or H···H bonding interaction.[18–22] One of the most accepted explanations is that the difference between the stabilities is due to a more effective π-bonding interaction in phenacenes. Local rings in phenacenes are more aromatic than in acenes, thus showing that the property that drives the greater stability of the phenacenes with respect to the acenes in the ground state is aromaticity. Their results are related to Clar's π-sextet model as phenanthrene has two aromatic π-sextets while anthracene has only one migrating π-sextet. Interestingly, dicationic linear anthracene is more stable than dicationic kinked phenanthrene by about 16 kcal.mol^{-1}.[23] But the dicationic anthracene has two π-sextets, the same number as dicationic phenanthrene. Therefore, if aromaticity is similar, the linear isomers are more stable than the kinked because the latter suffer from H···H repulsions in the bay regions of phenacenes.[24]

Beyond classical counting rules, several strategies and indicators have been developed to not only determine the (anti)aromatic character of a system, but also to quantify it.[25–27] There is a plethora of indicators of aromaticity that are based on different magnetic,[28] geometric,[29] electronic,[30] reactivity,[31,32] and orbital localization properties,[33] and more recently also derived from the information-theoretic approach.[34] However, the first three are the most popular and used criteria to quantify aromaticity.

For the case of excited states, specifically the lowest-lying triplet state, Hückel's rule is replaced by Baird's rule,[35] which is basically the inverse form of the first one. This rule states that a monocyclic conjugated compound is aromatic (antiaromatic) if it contains 4n (4n+2) π-electrons. The use of both rules (i.e. Hückel and Baird) has led to the development of design

strategies for the modulation of the photoelectronic properties of diverse compounds with potential technological applications.[36–39] However, for the study of PAHs in excited states, there are no known rules analogous to those proposed by Clar. To the best of the authors' knowledge, there are only a few studies in which the aromaticity of PAHs in the excited states has been explored,[39–46] so we consider necessary to make an exhaustive evaluation of local aromaticity in representative PAHs such as acenes and phenacenes.

The present article is aimed at the analysis of (anti)aromaticity in the lowest-lying triplet (π-π^*) T_1 state of a series of acenes and phenacenes using some of the most popular criteria of aromaticity, namely, magnetically induced current density (MICD),[47] out-of-plane component of the nucleus independent chemical shift ($NICS_{zz}$) at 0 and 1 Å above the molecular plane,[25,48,49] harmonic oscillator model of aromaticity (HOMA),[50] multicenter index (MCI),[51] *para*-delocalization index (PDI),[52] and aromatic fluctuation index (FLU).[53] We are aware that the impact of the T_1 state in the photochemistry of acenes and phenacenes is marginal compared to that of the S_1 state.[54–57] We focus on the T_1 state for three reasons: first, Baird's rule applies primarily to the T_1 state, second, the aromaticity of the T_1 and S_1 states is usually quite similar,[58] and, third, the S_1 state in acenes has an intrinsic multiconfigurational character that makes its study cumbersome especially for large acenes,[59–61] while T_1 states are well-described with unrestricted methods.[62]

Computational Methods

All structures studied in this work have been optimized without symmetry restrictions at the UB3LYP[63–65]/6-311G(d,p)[66,67] level using Gaussian 16 computational package.[68] It has been ensured that all compounds are minima in the potential energy surface through vibrational frequency calculations. Since PAHs have a biradical character as the number of rings

increases, the broken symmetry approach has been applied to study the singlet state for n ≥ 7.[69,70] To evaluate the reliability of the results obtained, single-triplet gaps were obtained and compared with experimental values reported in the literature. The magnetic criterion of aromaticity has been assessed through the Gauge Independent Atomic Orbital (GIAO) method in gas phase[71] using $NICS_{zz}$ at 0.0 and 1.0 Å above the molecular plane and in the center of each ring of the polycycle. Additionally, vector maps of magnetically induced current density (MICD) at 1 a.u. above the molecular plane are reported using the VisIt program.[72] For MICD calculations, an external B field was placed perpendicular to the molecular plane of the molecules. This magnetic field generates an electron movement and a ring current in accordance with the Biot-Savart law.[73] The GIAO-CD (GIAO Current Density) method proposed by Keith[74] have been applied for MICD calculation. This method allows to obtain current densities directly from the GIAO results in the context of the Quantum Theory of Atoms in Molecules[75] developed by Bader and implemented in AIMALL software.[76] On the other hand, the delocalization criteria have been tested using the MCI, PDI, and FLU using the ESI-3D program[77,78] in conjunction with the QTAIM space partitioning performed with AIMAll.[76] The evaluation of aromaticity with geometric criteria has been done using HOMA, which involves the measurement of the bond distance and equalization deviation of the ideal aromatic benzene molecule. Finally, the spin density was depicted using the Multiwfn[79] and Chemcraft programs[80] and numerically obtained through NBO calculations.[81] All indices of aromaticity have been obtained with the UB3LYP/6-311G(d,p) method.

Results and discussion

Studied acenes and phenacenes and their respective geometrical parameters are show in Figures 1 and S1 – S9 respectively. $\langle S^2 \rangle$ values close to 2.00 in Table S1 show that spin

contamination in the T_1 state of our systems is low and the obtained wavefunctions are appropriate in the description of this state in these systems. Furthermore, Mulliken spin densities at the DFT and CCSD(T) level have been compared for those n = 3 - 5 systems in the triplet state (see Table S2). The results show a reasonable correlation, supporting our calculations. This conclusion has been reinforced by T_1 test calculations performed at the CCSD(T) level for systems with n = 3 - 5 (see Table S3). Additionally, singlet-triplet energy gaps have been computed for acenes and phenacenes. For phenacenes and acenes with $n < 7$, we have considered the closed-shell singlet state as the ground state. For higher acenes (ca. $n \geq 7$), the ground state has an open-shell singlet character[59,60,69,82] or even polyradical character.[83] For acenes with $n \geq 7$, the open-shell singlet is the ground state at the UB3LYP/6-311G(d,p) level of theory. For *p*-benzyne, the open-shell singlet-triplet energy gap obtained at the B3LYP/6-31G(d) level of theory is of similar quality than that obtained with the CASPT2/cc-pVDZ method when compared to the experimental result.[68] Therefore, the UB3LYP/6-311G(d,p) singlet-triplet energy gaps (ΔE_{S-T}) are deemed to be reliable.

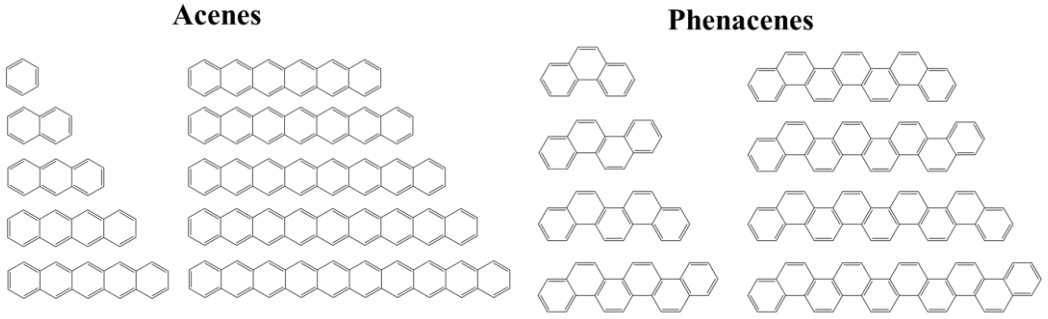

Figure 1. Structures of polycyclic aromatic hydrocarbons studied in this work.

Table 1 shows that our singlet-triplet energy gaps (ΔE_{S-T}) of [n]acenes are in good agreement with experimental data reported in the literature and calculations at the CCSD(T) level.[82,84] It is interesting to observe that in the case of acenes the value of ΔE_{S-T} decreases as the

number of six membered rings (6MR) increases. Benzene (Ac1) and naphthalene (Ac2) have the highest values (84.0 and 59.2 kcal.mol^{-1} respectively) while for Ac8 to Ac10 it is observed that the triplet state is less stable than the open-shell singlet state by only 5.0 kcal.mol^{-1}. These results indicate that in the acenes, the triplet state is becoming more and more stable as a 6MR is added up to n = 10, after that, the value of ΔE_{S-T} increases again, for n = 15 the value is 13.5 kcal.mol^{-1} (see Table S4 in SI). Phenacenes present larger deviations of ΔE_{S-T} from the experimental reports and CCSD(T) calculations, although the agreement is still acceptable. ΔE_{S-T} values are also reduced for the largest members of the series, however to a lesser degree with respect to acenes, so it is possible to state that triplets are less stable than singlets for the whole series.

Table 1. ZPE-corrected singlet-triplet energy gaps (in kcal.mol^{-1}) of acenes and phenacenes at the UB3LYP/6-311G(d,p) level. Experimental values are taken from refs. 82 and 84. Values in parentheses show the results obtained at the CCSD(T)/6-311G(d,p)///UB3LYP/6-311G(d,p) level.

Acenes	ΔE_{S-T}	ΔE_{S-Texp}	Phenacenes	ΔE_{S-T}	ΔE_{S-Texp}
Ac1	84.0 (90.3)	84.3	-	-	-
Ac2	59.2 (65.1)	60.9; 61.0	-	-	-
Ac3	39.6 (46.3)	42.6; 43.1	Ph3	60.5 (69.9)	61.5
Ac4	26.0 (33.6)	29.5; 29.3	Ph4	55.3 (65.7)	60.9
Ac5	16.5 (24.6)	19.8	Ph5	55.9 (70.4)	46.5
Ac6	9.5	12.4	Ph6	55.1	42.5
Ac7	6.8	-	Ph7	54.9	-
Ac8	5.4	-	Ph8	54.7	-
Ac9	5.0	-	Ph9	54.7	-
Ac10	5.3	-	Ph10	54.7	-

As commented before, several studies show that kinked PAHs (phenacenes) are more stable than their straight isomers (acenes). This result is confirmed by our results showed in Table 2. Additionally, it is possible to note that in the closed-shell singlet state, the addition of a

6MR leads to a periodic destabilization of approximately 5 kcal.mol^{-1} of the acenes with respect to the phenacenes (see Table 2). By a linear adjustment of least squares, it is possible to determine an empirical equation that allows predicting ΔE_{rel} in the closed-shell singlet state (see Figure S10 in SI). On the other hand, in the triplet state, relative energies show a different pattern, where acenes are more stable than their corresponding phenacene isomers up to 12 rings, while from 13 onwards, the phenacenes are again the most stable. The relative energies can be predicted through a quadratic adjustment which can be seen in Figure S10 in the SI. Additionally, energy differences between the triplet vertical (at the geometry of the closed-shell singlet) and adiabatic states of the phenacenes have been computed to quantify the stabilization due to loss of planarity of phenacenes in the T_1 state. The results in Table 2 show a constant energy difference of about 10 kcal.mol^{-1} between adiabatic and vertical T_1 states, which will be discussed in detail later.

Table 2. Relative energies (in kcal.mol^{-1}) between phenacenes and acenes in their singlet ground states and triplet states and relaxation energy for phenacenes at the UB3LYP/6-311G(d,p) level. ΔE_{rel} calculated as $E_{Acene} - E_{Phenacene}$ and ΔE_{relax} as $E_{ver\text{-}T} - E_T$.

PAHs	Singlet	Triplet	
N° rings	ΔE_{rel}	ΔE_{rel}	ΔE_{relax}
3	4.80	-16.09	10.48
4	9.63	-19.67	9.20
5	15.60	-23.83	10.19
6	21.88	-23.70	9.07
7	25.94	-22.18	9.68
8	30.04	-19.26	9.41
9	34.03	-15.61	9.59
10	38.10	-11.30	9.33
11	42.24	-6.55	9.54
12	46.44	-1.69	9.52
13	50.64	2.81	9.53
14	54.85	12.05	9.54
15	59.04	17.92	9.53

The change in stability trends is related to the loss of planarity of the phenacenes in the triplet state due to changes in the aromaticity of the 6MRs. The study of local aromaticity in both singlet and triplet states have been carried out using multiple indexes based on magnetic, electronic, and geometric properties. As mentioned above, regarding PAHs in the closed-shell singlet ground state, Poater et al.[24] showed that the differences in stability of anthracene (Ac3) and phenanthrene (Ph3) are due to the fact that the latter presents two aromatic rings located at the ends, while anthracene presents only a migrating sextet, according to Clar's rules. Figure 2a lists MCI values for Ac3 (Anthracene) and Ph3 (Phenanthrene) that confirm the previous reported results showing that the outer rings at Ph3 are more aromatic than the Ac3 rings. However, for the case of the triplet state, the story is different. In the triplet state, the outer rings in Ac3 retain similar MCI values, whereas the central ring has close to zero values. In addition, MICD vector maps (Figure 2b) show a strong paratropic (anticlockwise) ring current in the central ring in agreement with their antiaromatic behavior, whereas the outer rings show diatropic currents at the ring borders and paratropic currents inside them, a typical behavior of aromatic rings.[85] The paratropic current in the central ring is stronger because is reinforced by the diatropic currents of the outer rings due to the direction of the vectors. Figure S11 gathers the values of computed $NICS_{zz}$ descriptors, delocalization indexes, and HOMA confirming that there is a remarkable reduction in the aromaticity of the central Ac3 rings in the triplet state and that the aromatic character of the outer rings is preserved. When the spin density of Ac3 in the triplet state is plotted (Figure 2c), it is possible to observe that the electrons are preferentially located in the central ring in *para*-carbons 9 and 10. Ac3 can be described as a diradical antiaromatic Baird π-doublet located in the central ring and two aromatic Hückel π-sextets in the external rings (Figure 2d, left) or a diradical antiaromatic Baird π-tetradectet delocalized through the whole molecule.

Regarding Ph3 in its T_1 state, the three rings present paratropic currents being stronger in the central ring showing antiaromatic behavior. MCI values indicate that the aromaticity of the external rings are reduced by up to 40% as compared to the same rings in the ground state, while the central ring presents a high concentration of spin density (Figure 2c, right) and MCI values close to zero indicating antiaromatic character. Other computed aromaticity descriptors confirm these findings (see Figure S12). The reason (see Figure 2d) for the greater stability of Ac3 with respect to Ph3 in their T_1 states is twofold: 1) the outer rings in Ac3 are more aromatic, whereas in Ph3 these rings are weakly aromatic and 2) the presence of a H···H repulsion in the bay region of Ph3 destabilizes it by ca. 5 kcal.mol^{-1}.[24]

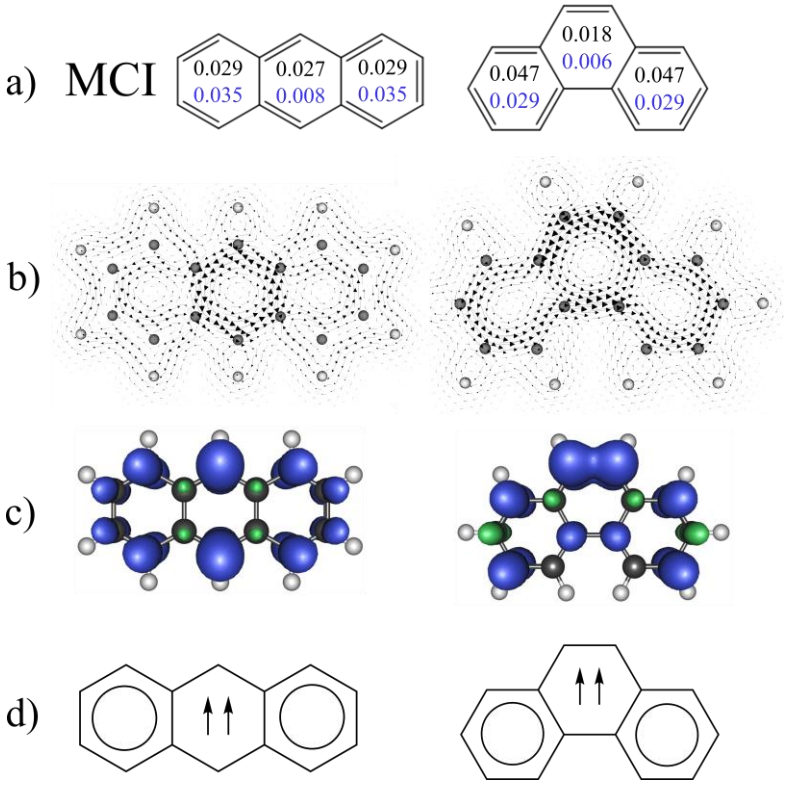

Figure 2. a) MCI values (units in e^-) in singlet (black) and triplet (blue) states for anthracene and phenanthrene. b) Magnetically induced current density vector maps, c) spin density plots (isosurface of ±0.005 a.u.) in triplet state for both compounds and d) Aromaticity/antiaromaticity schemes for anthracene and phenanthrene in their triplet states.

When the number of rings in the PAHs increases (n > 3) the spin density in the acenes is mostly located in the central ring(s) (Figure 3a and Figure S13), while the outer rings show low contribution from the spin density. Figure 3b and Figure S14 in SI shows the MCI values of acenes n = 4 – 10. The central rings in the triplet state present values close to zero (blue), while in the case of the outer rings they present similar or higher values to those in the singlet state, showing that the aromatic behavior of outer rings is preserved, and the central rings become antiaromatic. The remaining indicators based on the electron delocalization criterion support the remarkable variation of the aromaticity of the central ring and the conservation of the property in the outer rings. The results can be seen in Figures S15 – S17 in the SI.

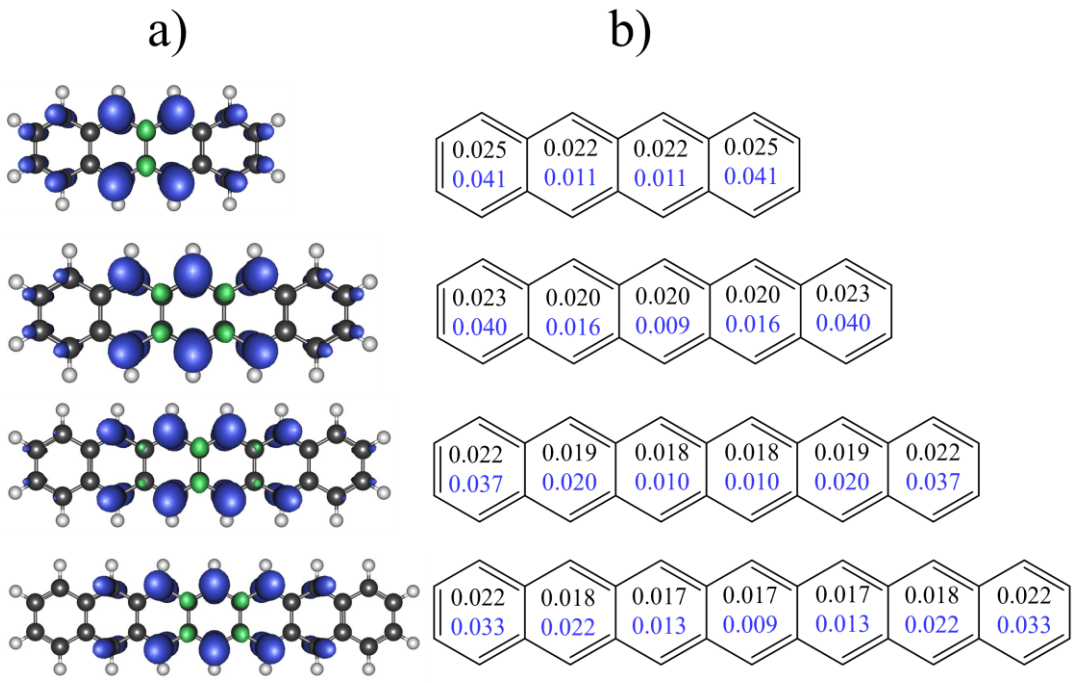

Figure 3. a) Spin density isosurfaces and b) MCI values of acenes (n = 4 – 7) in singlet (black) and triplet (blue) states at the UB3LYP/6-311G(d,p) level.

Additionally, the magnetic criteria through the MICD maps (Figure 4a and Figure S18 in SI) and $NICS_{zz}$ values (see Figures S19 and S20 in SI) show that the outer rings of the acenes in triplet state present diatropic ring currents in accordance with their aromatic behavior, while

the central rings show paratropic ring currents in agreement with the delocalization criteria shown previously. Figure 4b shows a scheme that describes the aromaticity of the [4]acene in the triplet state, where the outer rings retain their aromaticity and present two π-sextets while the central rings become a diradical antiaromatic Baird π-sextet. In the case of acenes with an odd number of rings, these present a delocalized pattern in form of π-doublets, π-dectects, and π-octadectets (Figure 4b), whereas in even (n > 4) acenes, the patterns are presented in the form of antiaromatic π-sextets and π-tetradectets.

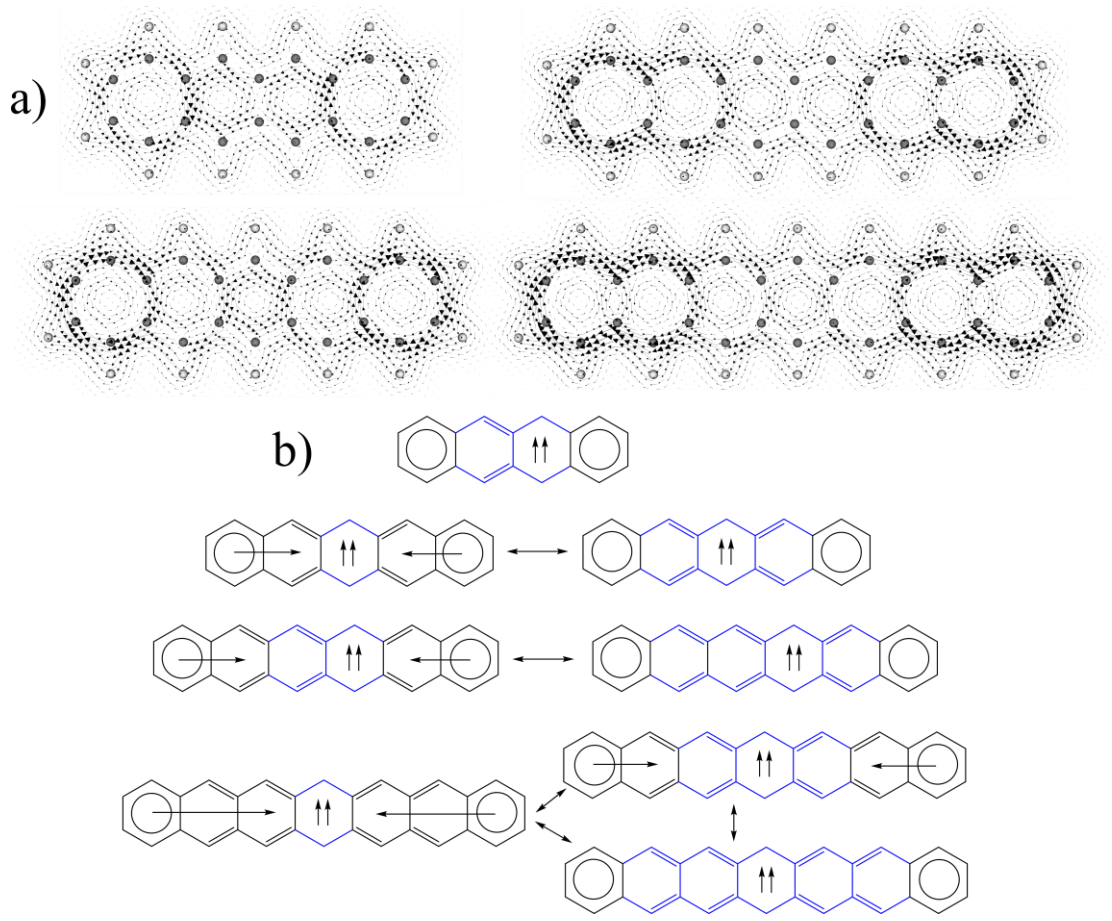

Figure 4. a) Magnetically induced current density vectorial maps for [n]acenes (n = 4 – 7) at the triplet state and b) schemes which best describe their (anti)aromatic behaviour.

The respective normalized weights of antiaromatic resonant structures have been obtained from the sum of the spin density values obtained from the NBO analysis of the carbon atoms

(see SI for full details). The results gathered in Table 3 numerically confirm the above. The highest amount of spin density is located in the form of the largest diradical, presenting contributions from 63 to 86% (for n > 4, see Table 3). In the cases of [7]acene and [9]acene, which have intermediate diradicals, these also have larger contributions than the smaller ones. We found that acenes prefer to delocalize spin density resulting in two aromatic Hückel islands in the outer rings and in the formation of the largest antiaromatic diradical Baird islands, thus providing an alternative explanation to that reported by Gershoni-Poranne et al.[62] It is worth noting that biphenylene in its T1 state shows an Baird aromatic π-dodected instead of a π-octet or π-quartet.[39]

Table 3. Estimation of weights for antiaromatic Baird's π-doublets, π-sextets, π-dectets, π-tetradectets, and π-octadectets in [n]acenes in their T_1 state.[a]

[n]Acene	Doublet	Sextet	Dectet	Tetradectet	Octadectet
3	100	-	-	-	-
4	-	100	-	-	-
5	14	-	86	-	-
6	-	29	-	71	-
7	7	-	35	-	58
8	-	21	-	79	
9	5	-	28	-	67
10	-	37	-	63	-

[a] See SI for the description of the method used.

On the other hand, concerning the phenacenes, the spin density distribution (Figure 5a and S21) is less homogeneous and is mostly located in the central rings that become antiaromatic, whereas the outer rings retain the aromaticity they had in the ground state. When analyzing the MCI values in the triplet state (Figure 5b, Figure S22), it is possible to observe that aromaticity is mostly affected in central rings. This behavior is maintained when observing the other computed geometrical and delocalization indicators (see Figures S23 – S25). Due

to the loss of symmetry and planarity, it is not possible to obtain vectorial maps of MICD, so to have more detail of the antiaromaticity through the magnetic criterion and to understand the deformation of these compounds, we have analyzed the MICD plots of the vertical triplet states of phenacenes.

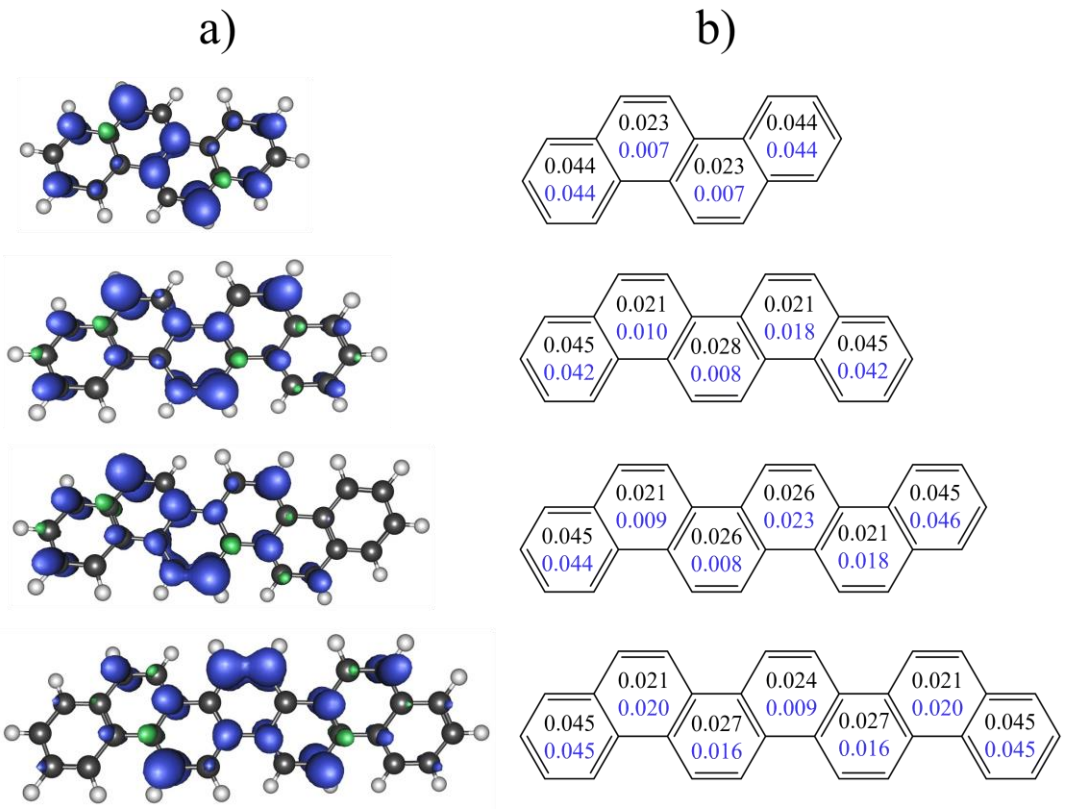

Figure 5. a) Spin density isosurfaces and b) MCI values of for phenacenes (n = 4 – 7) in singlet (black) and triplet (blue) states at the UB3LYP/6-311G(d,p) level in their adiabatic T_1 states.

Figures 6a and S26 show the vector maps of the vertical triplet state of phenacenes. As can be seen, the central rings present strong paratropic currents, while the outer rings present very weak currents. These results are similar to those obtained for the triplet adiabatic state (see Figure S27). The aromaticity pattern that allows explaining the vertical triplet state is the one observed in Figure 6b.

The outer rings retain their aromatic character in the form of aromatic Clar π-sextets, while the central rings possess an antiaromatic character and exhibit the behavior of diradical antiaromatic Baird π- sextet or π-dectet.

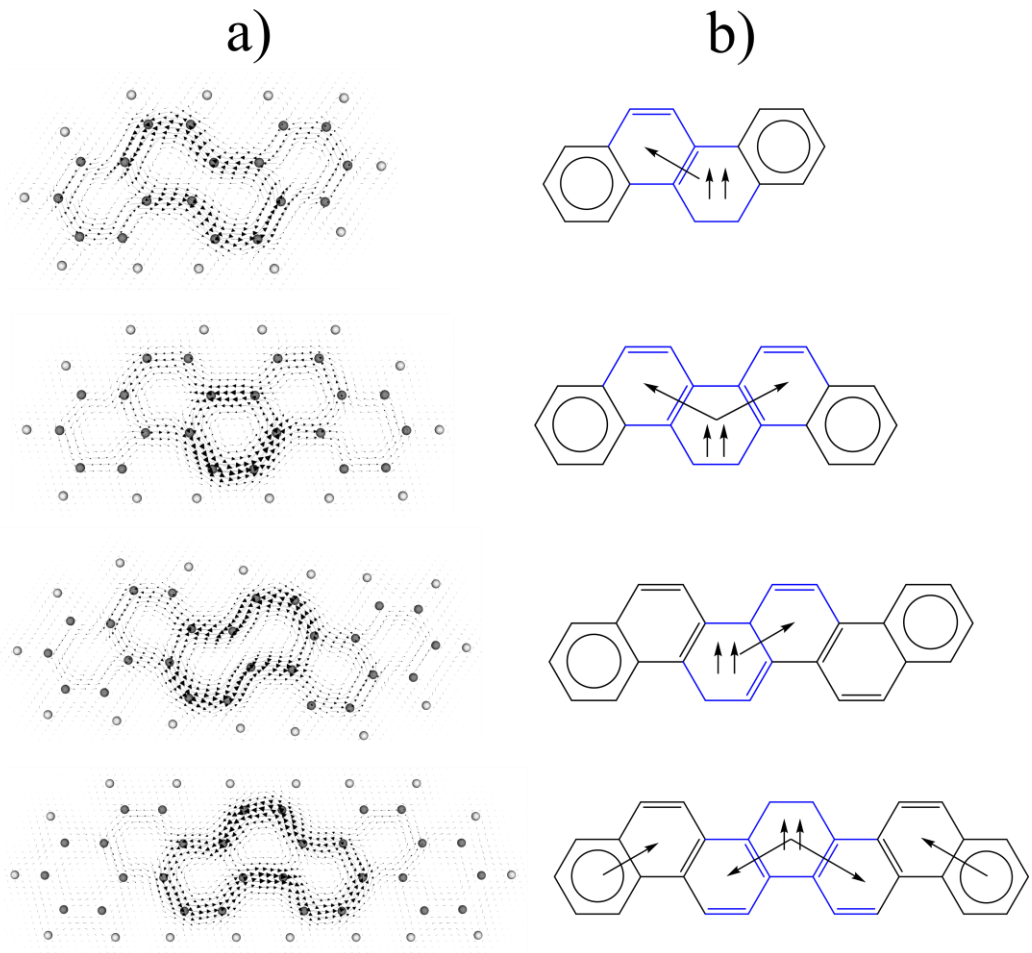

Figure 6. a) Magnetically induced current density vectorial maps for phenacenes (n = 4 – 7) at the vertical triplet state and b) Clar structures which best describe their (anti)aromatic behavior.

It has been shown that for the vertical triplet state the antiaromatic rings are symmetrically located in the center of the compound, while for the adiabatic state these are located in the second, third, fourth or fifth rings as can be seen in Figure 7. These differences can be attributed to the loss of symmetry due to the loss of planarity of the phenacenes, however, what explains these geometrical changes in the T_1 states of phenacenes?

The results of MCI in the vertical triplet state show similar values to the MCI of the adiabatic state (see Figure S27 in SI) so it is possible to indicate that the antiaromaticity is not the driving force that leads to the loss of planarity. On the other hand, as mentioned previously, the relaxation energy (ΔE_{relax}) of the triplet vertical and adiabatic states is about 10 kcal.mol^{-1} (Table 2). These energies can be explained by taking into account the H···H repulsion.[24] Figure 7 (in red) shows the effect of two steric repulsions between the hydrogen atoms for [n]phenacenes with n = 4 and 10, which leads to this molecule losing its planarity. Previous studies have reported that this repulsion destabilizes the molecule by approximately 5 kcal.mol^{-1}.[24] The relaxation energy for chrysene is 9.2 kcal.mol^{-1} according to the two repulsions shown. The same can be extrapolated to the rest of the phenacenes studied, where release of two H···H repulsions explains the loss of planarity of the systems. The relaxation energy values for the rest of the systems are found around 9 - 10 kcal.mol^{-1} allowing to suggest that the driving force that leads to the loss of symmetry of these systems is the steric H···H repulsion. Additionally, Figure 6 (right) shows that the aromatic pattern for phenacenes in the triplet state is composed of pairs of outer aromatic π-sextets while the central rings (in blue color) present an antiaromatic character, according to the results of MICD, MCI, and the rest of computed descriptors. The distortion from planarity disfavors electronic delocalization and, consequently, occurs around the antiaromatic central rings because the energy penalty charged is minimal in this case.[24] Rings with largest spin density are also the most Baird antiaromatic.[62,86]

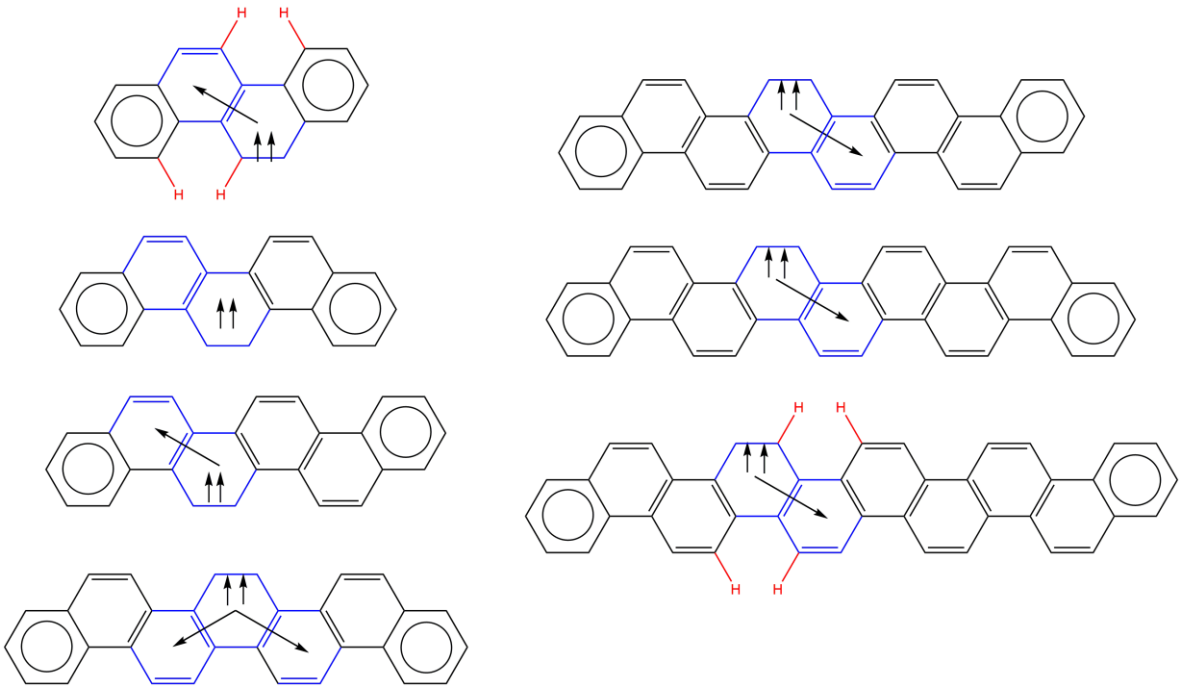

Figure 7. Aromaticity patterns for [n]phenacenes (n = 4 – 10) in the first adiabatic triplet state according to MCI calculations. Red bonds represent some H···H repulsions.

The (anti)aromaticity patterns for acenes and phenacenes in the triplet adiabatic state have serious consequences on their relative stability. In the case of acenes, they have antiaromatic rings in the central position and the outer rings retain their aromaticity in the form of two Clar π-sextets. Additionally, it is observed that planarity of this family is preserved. On the other hand, the aromaticity pattern in the triplet state of phenacenes shows that the antiaromatic rings are in most of the cases in the third and fourth positions, while the most outer rings retain their aromaticity in form of aromatic π-sextets. The rest of the rings show delocalization values that allow them to be assigned as non-aromatic. Additionally, it has been shown that the loss of planarity is due to the H···H repulsion of the antiaromatic rings with those next to them (see Figure 7). These differences also explain the trend in the relative stabilities of phenacenes with respect to acenes. However, when the systems gain more rings a second resonant structure becomes more relevant, as can be seen for the [8]phenacene in

Figure 8. For this reason, for n = 12 onwards and for the T_1 state, the phenacenes become again more stable than the acenes. We believe that the proposed Clar structures are a good representation of the (anti)aromaticity patterns in both vertical and adiabatic triplet states.

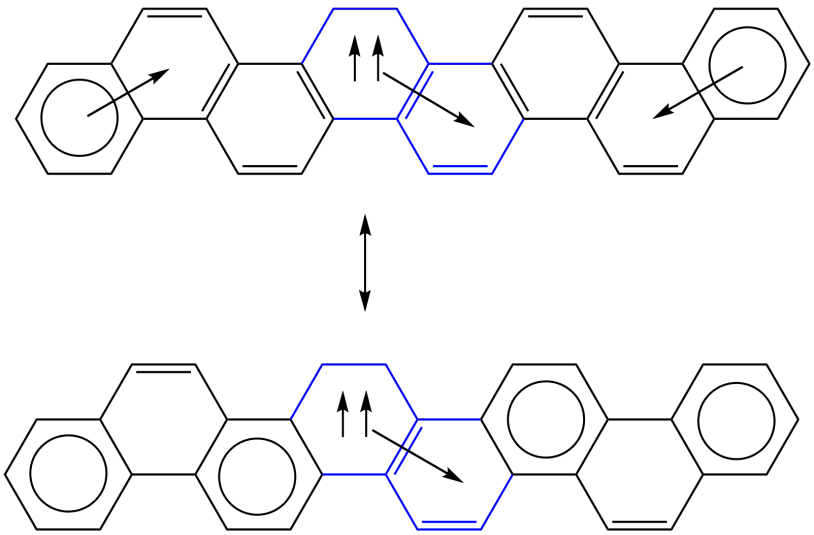

Figure 8. Most relevant Clar structures for describing aromaticity of [8]phenacene in the triplet state.

Conclusions

An exhaustive analysis of the stability and local aromaticity of the 6MR in acenes and phenacenes in their lowest-lying triplet state has been performed using multiple descriptors based on magnetic, delocalization, and geometric criteria. The results show similarities and differences between the vertical and adiabatic states studied. The vertical and adiabatic triplet states in acenes show that the central rings present an antiaromatic character in the form of a combination of diradical antiaromatic Baird π-doublets, π-sextets, π-dectets, π-tetradectets or π-octadectets, while the outer rings retain their aromaticity in the form of traditional Clar π-sextets. The pattern shown for the vertical and adiabatic T_1 states is the same since the system

retains its planarity. For phenacenes in their vertical triplet state, the central rings become diradical antiaromatic Baird π-sextets or π-dectets, while the external rings are aromatic in the form of Clar π-sextets. On the other hand, the triplet adiabatic state presents a remarkable loss of planarity which is translated into a change in the aromaticity pattern. The antiaromatic Baird π-sextets are no more in the central positions due to the loss of symmetry. The differences in the aromaticity of the vertical and adiabatic states for phenacenes are due to H···H repulsions like those observed in the singlet state, generating a change in the aromatic pattern of this family of compounds. Additionally, changes in relative stability between phenacenes and acenes are related to aromaticity patterns. In the T_1 state, the acenes are more stable because they have the same number of aromatic π-sextets as phenacenes, but they do not suffer from H···H repulsions. However, when the number of rings increases, the phenacenes become more stable again. This is because a second resonant structure that present additional localized aromatic Clar π-sextets becomes more important, stabilizing the phenacenes. The shown representations provide a clear understanding of the changes in aromaticity of [n]acenes and [n]phenacenes in their triplet state.

Acknowledgements

R.B-G. is grateful for the financial support of FONDECYT Postdoctorado 3210037. Powered@NLHPC. This research was partially supported by the supercomputing infrastructure of the NLHPC (ECM-02). M.S. acknowledges the financial support from the Ministerio de Economía y Competitividad of Spain (project CTQ2017-85341-P) and the Generalitat de Catalunya (project 2017SGR39).

Supplementary Information

Detailed computed aromaticity descriptors, MICD vector maps, spin density isosurfaces, T_1 test results, and Cartesian coordinates for all systems studied in this work.

References

1 P. v. R. Schleyer, *Chem. Rev.*, 2001, **101**, 1115–1118.

2 Y. M. Sung, M.-C. Yoon, J. M. Lim, H. Rath, K. Naoda, A. Osuka and D. Kim, *Nat. Chem.*, 2015, **7**, 418–422.

3 M. Ueda, K. Jorner, Y. M. Sung, T. Mori, Q. Xiao, D. Kim, H. Ottosson, T. Aida and Y. Itoh, *Nat. Commun.*, 2017, **8**, 346.

4 W.-Y. Cha, T. Kim, A. Ghosh, Z. Zhang, X.-S. Ke, R. Ali, V. M. Lynch, J. Jung, W. Kim, S. Lee, S. Fukuzumi, J. S. Park, J. L. Sessler, T. K. Chandrashekar and D. Kim, *Nat. Chem.*, 2017, **9**, 1243–1248.

5 H. Ottosson, *Nat. Chem.*, 2012, **4**, 969–971.

6 S. Escayola, C. Tonnelé, E. Matito, A. Poater, H. Ottosson, M. Solà and D. Casanova, *Angew. Chemie Int. Ed.*, 2021, **60**, 10225-10265.

7 W. Zeng, O. El Bakouri, D. W. Szczepanik, H. Bronstein and H. Ottosson, *Chem. Sci.*, 2021, **12**, 6159–6171.

8 M. Solà, *WIREs Comput. Mol. Sci.*, 2019, **9**, e1404.

9 E. Hückel, *Zeitschrift für Phys.*, 1931, **72**, 310–337.

10 E. Clar, The Aromatic Sextet, Wiley, New York, 1972

11 M. Solà, *Front. Chem.*, 2013, **1**, 22.

12 C. Glidewell and D. Lloyd, *Tetrahedron*, 1984, **40**, 4455–4472.

13 H. Okamoto, *Phys. Chem. Carbon-Based Mater. Basics Appl.*, 2019, 211–228.

14 C. Tönshoff and H. F. Bettinger, *Chem. Eur. J.*, 2020, **27**, 3193-3212.

15 J. Poater, R. Visser, M. Solà and F. M. Bickelhaupt, *J. Org. Chem.*, 2007, **72**, 1134–1142.

16 A. Ciesielski, T. M. Krygowski and M. K. Cyrański, *J. Chem. Inf. Model.*, 2008, **48**, 1358–1366.

17 L. Pauling and J. Sherman, *J. Chem. Phys.*, 1933, **1**, 606–617.

18 C. F. Matta, J. Hernández-Trujillo, T.-H. Tang and R. F. W. Bader, *Chem. Eur. J.*, 2003, **9**, 1940–1951.

19 D. S. Sabirov, *Comput. Theor. Chem.*, 2014, **1030**, 81–86.

20 A. M. Pendás, E. Francisco, M. A. Blanco and C. Gatti, *Chem. Eur. J.*, 2007, **13**, 9362–9371.

21 A. V Vashchenko and T. N. Borodina, *J. Struct. Chem.*, 2013, **54**, 479–483.

22 D. J. Wolstenholme and T. S. Cameron, *J. Phys. Chem. A*, 2006, **110**, 8970–8978.

23 J. Dominikowska and M. Palusiak, *Phys. Chem. Chem. Phys.*, 2011, **13**, 11976–11984.

24 J. Poater, M. Duran and M. Solà, *Front. Chem.*, 2018, **6**, 561.

25 R. Báez-Grez, L. Ruiz, R. Pino-Rios and W. Tiznado, *RSC Adv.*, 2018, **8**, 13446–13453.

26 R. Báez-Grez, W. A. Rabanal-León, L. Alvarez-Thon, L. Ruiz, W. Tiznado and R. Pino-Rios, *J. Phys. Org. Chem.*, 2018.

27 R. Báez-Grez and R. Pino-Rios, *New J. Chem.*, 2020, **44**, 18069–18073.

28 R. Gershoni-Poranne and A. Stanger, *Chem. Soc. Rev.*, 2015, **44**, 6597–6615.

29 T. M. Krygowski and M. K. Cyrański, *Chem. Rev.*, 2001, **101**, 1385–1420.

30 F. Feixas, E. Matito, J. Poater and M. Sola, *Chem. Soc. Rev.*, 2015, **44**, 6434–6451.

31 Z. Mucsi, B. Viskolcz and I. G. Csizmadia, *J. Phys. Chem. A*, 2007, **111**, 1123–1132.

32 R. Pino-Rios, D. Inostroza, G. Cárdenas-Jirón and W. Tiznado, *J. Phys. Chem. A*, 2019, **123**, 10556–10562.

33 D. Y. Zubarev and A. I. Boldyrev, *Phys. Chem. Chem. Phys.*, 2008, **10**, 5207–5217.

34 D. Yu, T. Stuyver, C. Rong, M. Alonso, T. Lu, F. De Proft, P. Geerlings and S. Liu, *Phys. Chem. Chem. Phys.*, 2019, **21**, 18195–18210.

35 N. C. Baird, *J. Am. Chem. Soc.*, 1972, **94**, 4941–4948.

36 O. El Bakouri, J. R. Smith and H. Ottosson, *J. Am. Chem. Soc.*, 2020, **142**, 5602–5617.

37 M. Rosenberg, C. Dahlstrand, K. Kilså and H. Ottosson, *Chem. Rev.*, 2014, **114**, 5379–5425.

38 J. Malkin, Photophysical and Photochemical Properties of Aromatic Compounds,

CRC Press, Rehovot, 1992.

39 R. Ayub, O. El Bakouri, K. Jorner, M. Solà and H. Ottosson, *J. Org. Chem.*, 2017, **82**, 6327–6340.

40 C. Dahlstrand, M. Rosenberg, K. Kilså and H. Ottosson, *J. Phys. Chem. A*, 2012, **116**, 5008–5017.

41 K. Jorner, R. Emanuelsson, C. Dahlstrand, H. Tong, A. V Denisova and H. Ottosson, *Chem. Eur. J.*, 2014, **20**, 9295–9303.

42 M. Baranac-Stojanović, *J. Org. Chem.*, 2020, **85**, 4289–4297.

43 Z. Wen, L. J. Karas, C.-H. Wu and J. I.-C. Wu, *Chem. Commun.*, 2020, **56**, 8380–8383.

44 C.-H. Wu, L. J. Karas, H. Ottosson and J. I.-C. Wu, *Proc. Natl. Acad. Sci.*, 2019, **116**, 20303 LP – 20308.

45 B. J. Lampkin, Y. H. Nguyen, P. B. Karadakov and B. VanVeller, *Phys. Chem. Chem. Phys.*, 2019, **21**, 11608–11614.

46 J. C. Dobrowolski and G. Karpińska, *ACS Omega*, 2020, **5**, 9477–9490.

47 D. Sundholm, H. Fliegl and R. J. F. Berger, *Wiley Interdiscip. Rev. Comput. Mol. Sci.*, 2016, **6**, 639–678.

48 P. v. R. Schleyer, H. Jiao, N. J. R. van E. Hommes, V. G. Malkin and O. L. Malkina, *J. Am. Chem. Soc.*, 1997, **119**, 12669–12670.

49 I. Cernusak, P. W. Fowler and E. Steiner, *Mol. Phys.*, 2000, **98**, 945–953.

50 J. Kruszewski and T. M. Krygowski, *Tetrahedron Lett.*, 1972, **13**, 3839–3842.

51 P. Bultinck, R. Ponec and S. Van Damme, *J. Phys. Org. Chem.*, 2005, **18**, 706–718.

52 J. Poater, X. Fradera, M. Duran and M. Solà, *Chem. Eur. J.*, 2003, **9**, 400–406.

53 E. Matito, M. Duran and M. Solà, *J. Chem. Phys.*, 2004, **122**, 14109; Erratum íbid. 2006, *125*, 059901.

54 J. E. Anthony, *Chem. Rev.*, 2006, **106**, 5028–5048.

55 H. Okamoto, S. Hamao, R. Eguchi, H. Goto, Y. Takabayashi, P. Y.-H. Yen, L. U. Liang, C.-W. Chou, G. Hoffmann, S. Gohda, H. Sugino, Y.-F. Liao, H. Ishii and Y. Kubozono, *Sci. Rep.*, 2019, **9**, 4009.

56 Y. Shimo, T. Mikami, S. Hamao, H. Goto, H. Okamoto, R. Eguchi, S. Gohda, Y. Hayashi and Y. Kubozono, *Sci. Rep.*, 2016, **6**, 21008.

57 A. Al Ruzaiqi, H. Okamoto, Y. Kubozono, U. Zschieschang, H. Klauk, P. Baran and H. Gleskova, *Org. Electron.*, 2019, **73**, 286–291.

58 F. Feixas, J. Vandenbussche, P. Bultinck, E. Matito and M. Solà, *Phys. Chem. Chem. Phys.*, 2011, **13**, 20690–20703.

59 M. Bendikov, H. M. Duong, K. Starkey, K. N. Houk, E. A. Carter and F. Wudl, *J. Am. Chem. Soc.*, 2004, **126**, 7416–7417.

60 Y. Yang, E. R. Davidson and W. Yang, *Proc. Natl. Acad. Sci.*, 2016, **113**, E5098-E5107.

61 A. E. Torres, P. Guadarrama and S. Fomine, *J. Mol. Model.*, 2014, **20**, 2208.

62 G. Markert, E. Paenurk and R. Gershoni-Poranne, *Chem. Eur. J.*, 2021, **27**, 6923-6935.

63 C. Lee, W. Yang and R. G. Parr, *Phys. Rev. B*, 1988, **37**, 785–789.

64 A. D. Becke, *J. Chem. Phys*, 1993, **98**, 5648–5652.

65 P. J. Stephens, F. J. Devlin, C. F. N. Chabalowski and M. J. Frisch, *J. Phys. Chem.*, 1994, **98**, 11623–11627.

66 W. J. Hehre, R. Ditchfield and J. A. Pople, *J. Chem. Phys.*, 1972, **56**, 2257–2261.

67 R. Ditchfield, W. J. Hehre and J. A. Pople, *J. Chem. Phys.*, 1971, **54**, 724–728.

68 M. J. Frisch, G. W. Trucks, H. B. Schlegel, G. E. Scuseria, M. A. Robb, J. R. Cheeseman, G. Scalmani, V. Barone, G. A. Petersson, H. Nakatsuji, X. Li, M. Caricato, A. V. Marenich, J. Bloino, B. G. Janesko, R. Gomperts, B. Mennucci, H. P. Hratchian, J. V. Ortiz, A. F. Izmaylov, F. Egidi, J. Goings, B. Peng, A. Petrone, T. Henderson, D. Ranasinghe, V. G. Zakrzewski, J. Gao, N. Rega, G. Zheng, W. Liang, M. Ishida, T. Nakajima, Y. Honda, O. Kitao, H. Nakai, T. Vreven, K. Throssell, J. A. Montgomery, Jr., J. E. Peralta, F. Ogliaro, M. J. Bearpark, J. J. Heyd, E. N. Brothers, K. N. Kudin, V. N. Staroverov, T. A. Keith, R. Kobayashi, J. Normand, K. Raghavachari, A. P. Rendell, J. C. Burant, S. S. Iyengar, J. Tomasi, M. Cossi, J. M. Millam, M. Klene, C. Adamo, R. Cammi, J. W. Ochterski, R. L. Martin, K. Morokuma, O. Farkas, J. B. Foresman and D. J. Fox, *Gaussian 16, Revision B.01*, Gaussian, Inc., Wallingford CT, 2016.

69 J. Poater, J. M. Bofill, P. Alemany and M. Solà, *J. Phys. Chem. A*, 2005, **109**, 10629–10632.

70 J. Poater, F. M. Bickelhaupt and M. Solà, *J. Phys. Chem. A*, 2007, **111**, 5063–5070.

71 K. Wolinski, J. F. Hinton and P. Pulay, *J. Am. Chem. Soc.*, 1990, **112**, 8251–8260.

72 H. Childs, E. Brugger, B. Whitlock, J. Meredith, S. Ahern, D. Pugmire, K. Biagas, M. Miller, C. Harrison, G. H. Weber, H. Krishnan, T. Fogal, A. Sanderson, C. Garth, E. W. Bethel, D. Camp, O. Rübel, M. Durant, J. M. Favre and P. Navrátil, VisIt: An End-User Tool For Visualizing and Analyzing Very Large Data, *High Perform. Vis. Extrem. Sci. Insight*, 2012, 357–372.

73 D. C. Giancoli, Physics for Scientist & Engineers, Pearson Education International, 2008.

74 T. A. Keith, *Chem. Phys.*, 1996, **213**, 123–132.

75 R. F. W. Bader, Clarendon Press, 1994.

76 T. G. S. Todd A. Keith, *AIMAll (Version 19.02.13)*, Overland Park KS, EE. UU., 2019 (aim.tkgristmill.com).

77 E. Matito, ESI-3D: Electron Sharing Indices Program for 3D Molecular Space Partitioning; Institute of Computational Chemistry and Catalysis (IQCC), University of Girona, Catalonia, Spain, 2006; http://iqcc.udg.edu/ eduard/ESI.

78 E. Matito, M. Solà, P. Salvador and M. Duran, *Faraday Discuss.*, 2007, **135**, 325–345.

79 T. Lu and F. Chen, *J. Comput. Chem.*, 2012, **33**, 580–592.

80 Chemcraft - graphical software for visualization of quantum chemistry computations. (https://www.chemcraftprog.com), Chemcraft.

81 E. D. Glendening, J. K. Badenhoop, A. E. Reed, J. E. Carpenter, J. A. Bohmann, C. M. Morales, C. R. Landis and F. Weinhold, Natural bond orbital analysis program: NBO 6.0, *Theor. Chem. Institute, Univ. Wisconsin, Madison, WI*.

82 C. U. Ibeji and D. Ghosh, *Phys. Chem. Chem. Phys.*, 2015, **17**, 9849–9856.

83 G. Trinquier, G. David and J.-P. Malrieu, *J. Phys. Chem. A*, 2018, **122**, 6926–6933.

84 H. Okamoto, M. Yamaji, S. Gohda, K. Sato, H. Sugino and K. Satake, *Res. Chem. Intermed.*, 2013, **39**, 147–159.

85 H. Fliegl, D. Sundholm, S. Taubert, J. Jusélius and W. Klopper, *J. Phys. Chem. A*, 2009, **113**, 8668–8676.

86 R. Papadakis, H. Li, J. Bergman, A. Lundstedt, K. Jorner, R. Ayub, S. Haldar, B. O. Jahn, A. Denisova, B. Zietz, R. Lindh, B. Sanyal, H. Grennberg, K. Leifer and H. Ottosson, *Nat. Commun.*, 2016, **7**, 12962.

GRAPHIC FOR THE TABLE OF CONTENTS